Novel and ideal zirconium-based dense membrane reactors for partial oxidation of methane to syngas

Jianhua Tong, Weishen Yang *, Rui Cai, Baichun Zhu, and Liwu Lin

State Key Laboratory of Catalysis, Dalian Institute of Chemical Physics, Chinese Academy of Sciences, PO Box 110, Dalian, 116023, PR China

Received 21 June 2001; accepted 1 October 2001

A novel and ideal dense catalytic membrane reactor for the reaction of partial oxidation of methane to syngas (POM) was constructed from the stable mixed conducting perovskite material of $BaCo_{0.4}Fe_{0.4}Zr_{0.2}O_{3-\delta}$ and the catalyst of $LiLaNiO/\gamma\text{-}Al_2O_3$. The POM reaction was performed successfully. Not only was a short induction period of 2 h obtained, but also a high catalytic performance of 96–98% CH_4 conversion, 98–99% CO selectivity and an oxygen permeation flux of 5.4–5.8 $ml\,cm^{-2}\,min^{-1}$ (1.9–2.0 $\mu mol\,m^{-2}\,S^{-1}\,Pa^{-1}$) at 850 °C were achieved. Moreover, the reaction has been steadily carried out for more than 2200 h, and no interaction between the membrane material and the catalyst took place.

KEY WORDS: zirconium membrane; methane oxidation; syngas production

1. Introduction

The most effective application of the abundant natural gas in world was to convert methane to more useful and easily transported chemicals. The direct conversion approach was to produce methanol, formaldehyde, or olefins by partially oxidizing methane directly. This approach was too difficult to realize because the desired products of the reaction were more reactive than the starting reactant (CH_4). This eventually led to deep oxidation and high selectivity of CO_2 and H_2O [1]. The alternative conversion approach for methane was to produce syngas ($CO + H_2$) by partially oxidizing methane in the first stage, which could be achieved by either steam reforming or direct partial oxidation, or a combination of both. Then the syngas was converted into upgraded chemicals in the next stage by methanol synthesis or Fischer–Tropsch technology. But the commercially used method of steam reforming needed to operate at high temperatures and high pressures. The cost of syngas production by steam reforming was too high to apply this process into practice. So attention was turned to the process of the direct partial oxidation of methane to syngas (POM). Although POM has received increasing attention as an alternative method in recent years and many active catalysts with high CH_4 conversion, high CO selectivity and proper ratio of H_2 to CO have been reported [2–4], commercial-scale plants have not been realized up to now. The hot-spot problem of a conventional co-fed reactor for the exothermic POM reaction, which might result in reactor runway, had to be carefully dealt with in the reactor design. The design of the reactor was focused on how to remove the additional heat efficiently. For instance, the cyclic reactor [5], in which flow direction was periodically reversed for heat exchange, and the combined reactor, in which heat recovery from a second auto-thermal packed-bed reactor was provided for a primary steam reformer [6], were attempted. The second obstruction for the direct syngas production from the economic point was that air was usually used as oxidant. Since the downstream upgrading process required the syngas stream to be free from nitrogen and the by-production of NO_x, either N_2 or NO_x must be eliminated from the syngas stream, or oxygen must be separated from air (usually cryogenically) before being fed to the POM reactor. Although upstream oxygen separation from air was more favorable than the costly downstream purification, the conventional cryogenic oxygen plant was very costly in operation combined with the partial oxidation process. A novel catalytic membrane reactor, such as a mixed oxygen ion and electron membrane (MIECM) reactor, in which oxygen was separated from air and simultaneously fed into the methane stream without impairing the conversion and selectivity, was becoming an appreciated design.

The principle behind application of this MIECM reactor technology for the POM reaction is shown in figure 1. The MIECM was exclusively an oxygen ion and electron conductor, which behaved as short-circuited electrochemical cells with oxygen ions transporting from the oxygen-rich side to the oxygen-lean side of the membrane and electrons mediating in a contrary process *via* the membrane lattice bulk. Moreover, no electrical energy was required to drive that thermodynamically downhill process for the meaningless. Employing an MIECM reactor not only allowed the direct use of air as an oxidant, such that the product was free from the nitrogen impurity and the formation of NO_x during high-temperature reaction was avoided, but also could circumvent flammability limits due to the separation of oxidant and reductant. The hot-spot problem of the conventional co-fed reactor could also be avoided by the separate feeding of methane and oxygen by using MIECM reactors. In addition,

* To whom correspondence should be addressed. E-mail: yangws@dicp.ac.cn

1011-372X/02/0300-0129/0 © 2002 Plenum Publishing Corporation

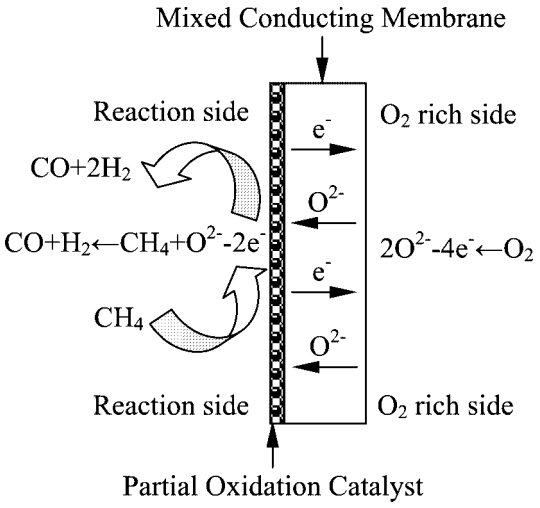

Figure 1. Schematic diagram of the mixed conducting membrane reactor for spontaneous partial oxidation of methane to syngas.

the cost of the gas compression in downstream processing could also be greatly reduced.

Recent reports in the literature suggested that the MIECM could successfully separate oxygen from air at a commercially feasible flux ($>1.0\,\mathrm{ml\,cm^{-2}\,min^{-1}}$) [7–15]. But when the MIECM was applied to the POM reaction, the high oxygen permeability, good chemical stability, high mechanical strength and good compatibility between membrane materials and catalysts would be supplied simultaneously. Due to this harsh demand, some membrane materials were not suitable for the reaction of POM. In order to resolve this problem the Zr^{4+} ion was selected in the present work to synthesize a perovskite structure oxide of $BaCo_{0.4}Fe_{0.4}Zr_{0.2}O_{3-\delta}$ (BCFZO) for the first time due to its high mechanical strength, low thermal conductivity and stability in the high valence state [16,17].

2. Experimental

2.1. Preparation of the catalyst and membrane disks

Powders of BCFZO and compared material of $SrCo_{0.8}Fe_{0.2}O_{3-\delta}$ (SCFO) were synthesized from nitrates of the component metals *via* a method of combining EDTA acid and citric complexes. In brief, the calculated amounts of nitrates were dissolved in EDTA-$NH_3{\cdot}H_2O$ ($NH_3{\cdot}H_2O$, 8 mol l^{-1}, EDTA : $NH_3{\cdot}H_2O$ = 1 g : 10 ml) solution under heating and stirring. Then a proper amount of citric acid was introduced, the mole ratio of EDTA acid : citric acid : total metal ions was controlled to be around 1 : 1.5 : 1. Precipitation might occur after the addition of citric acid, then $NH_3{\cdot}H_2O$ or HNO_3 was added to adjust the pH value to around 6, and the solution became transparent immediately. By evaporating the water, a dark purple gel was obtained. The gel was then heated at 120 °C for 10 h to get primary powders, which were calcined at 950 °C for 5 h to obtain powders with the final composition.

The as-synthesized powders were compressed into disks in a stainless-steel mold (17 mm in diameter) under hydraulic pressures of 15–25 MPa based on an area of 2.27 cm^2. Green disk compacts were then sintered in air at 1100–1200 °C for 10 h, with heating and cooling rates of 1 and 2 °C min^{-1}, respectively. The densities of the sintered membrane disks were determined by the Archimedes method using ethanol. Only those membrane disks that had relative densities higher than 95% were used for permeation study and constructing POM reactors.

LiLaNiO/γ-Al_2O_3 catalyst with 10 wt% nickel loading was prepared by the impregnation method [18]. Appropriate amounts of $LiNO_3$, $Ni(NO_3)_2$ and $La(NO_3)_3$ were co-impregnated on γ-Al_2O_3 supports. After drying at 120 °C for 24 h under an open environment, it was calcined in air at 550–800 °C for 4 h.

2.2. Characterization of the membrane materials

X-ray diffraction (XRD, Rigaku D-Max/RB) was used to characterize the structure of the powders and the membrane disks after treatment under different conditions. The samples of SCFO and BCFZO before and after O_2-TPD were submitted to XRD measurement for characterization of their structural stability under oxidizing and inert atmospheres. In order to check their structural stability under a more reducing atmosphere, the samples of SCFO and BCFZO after H_2-TPR (5% H_2 + 95% Ar) were recovered in a more oxidizing atmosphere (1% O_2 + 99% Ar) and then submitted to XRD characterization. The XRD patterns of BCFZO after treatment in pure helium at 650, 750, 850 and 950 °C for 100 h were acquired. In order to check the structure change of the membrane disk after long-term POM reaction, the two membrane surfaces after removing the top layers were also submitted to XRD characterization. SEM-EDS (JEM-5600LV, Oxford ISIS-300) and XPS (VG ESCA LABMKII) were used to characterize the interaction of the membrane disk and the LiLaNiO/γ-Al_2O_3 catalyst. The structural stability under inert and reducing atmospheres was characterized by techniques of oxygen programmed desorption (O_2-TPD) and hydrogen programmed reduction (H_2-TPR). The oxygen desorption experiment was performed according to the following procedure [13]. About 1 g of the sample was loaded in a quartz glass tube and treated in a pure oxygen atmosphere at 800 °C for 2 h. After the temperature was cooled down to room temperature at a rate of 1 °C min^{-1}, the oxygen desorption experiment was performed by increasing the temperature from 20 to 1020 °C at a rate of 10 °C min^{-1}. Highly pure He was used as the carrier gas, with a flow rate of 30 ml min^{-1}. A thermal conductivity detector (TCD) was used on line for signal detection with a computer data acquisition system. In order to examine the reversibility of oxygen adsorption and desorption, the sample after O_2-TPD was treated in pure oxygen atmosphere at 800 °C for 2 h, then cooled down to room temperature, as described above, and the O_2-TPD experiment was performed again. Compared with the procedure of O_2-TPD, the H_2-TPR experimental

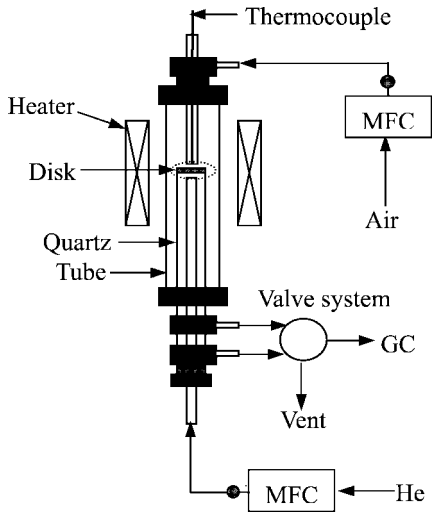

Figure 2. Schematic diagram of high-temperature permeation cell.

procedure had some differences, for example, the amount of sample was 60 mg rather than 1 g, the pretreatment atmosphere was a mixture of 1% O_2 and 99% Ar rather than pure oxygen and the carrier gas was a mixture of 5% H_2 and 95% Ar. After H_2-TPR, the sample was recovered with a flow of 1% O_2 and 99% Ar mixed gases at 800 °C for a certain time, then cooled down to room temperature quickly under the same atmosphere. The next-run H_2-TPR experiment was performed again. This process was repeated several times for obtaining multi-run H_2-TPR profiles.

2.3. Oxygen permeability under air/He gradient

The oxygen permeation experiments under an air/He gradient were performed in a vertical high-temperature gas permeation cell, as shown in figure 2. A ceramic glass powder (Keramik-Glasur, UHLIG, Germany) was used as the ceramic binding agent to seal the disk into a dense quartz tube. The sidewall of the disk was also covered with the paste based on the ceramic glass powder to avoid a radial contribution to the oxygen permeation flux. After assembly of the permeation cell, the temperature was increased up to 1040 °C at a heating rate of 2 °C min^{-1} and held at this temperature for 10 min. The ceramic glass powder was softened and it fused the membrane disk and the quartz tube. The permeation study was performed within the temperature range of 600–950 °C. An HP6890 gas chromatograph equipped with a 5A sieve column for the separation of O_2 and N_2 was connected to the exit of the oxygen-lean side. The gas chromatograph was frequently calibrated using standard gases of oxygen in helium in order to ensure reliability of the experimental data. The detailed experimental procedure and the calculation of oxygen permeation flux were given in [14].

2.4. Performance of the POM reaction

The membrane reactor configuration for the POM reaction is shown in figure 3. After polishing on both surfaces, the membrane disk was mounted on a quartz tube with a gold

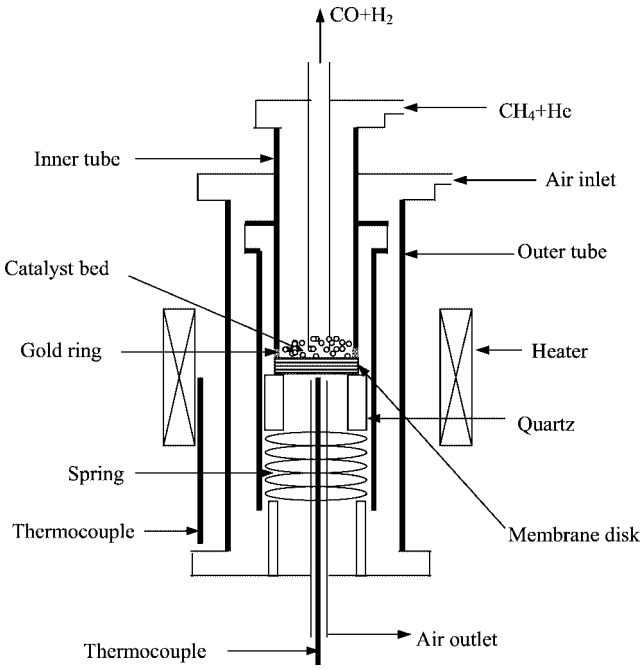

Figure 3. The configuration of the mixed conducting membrane reactor for partial oxidation of methane to syngas.

ring seal. Then the temperature was increased to 1070 °C and maintained at this temperature for several minutes. After sealing the membrane disk well, the temperature was cooled down to 850 °C at a rate of 1 °C min^{-1} and 300 mg of LiLaNiO/γ-Al_2O_3 catalyst containing 10% Ni prepared by impregnation [18] was loaded on the membrane surface. Then the diluted methane (50% He and 50% CH_4) and air were introduced to start the reaction. An HP6890 gas chromatograph equipped with a 5A molecular sieve column (for the separation of H_2, O_2, N_2, CH_4 and CO) and a TDX-01 column (for the separation of CO, CO_2 and hydrocarbons) were used for analyzing the compositions of the product gases. The total flow rates at the inlet and outlet of the reactor were separately measured by a soap flow meter. Methane conversion, CO selectivity, CO_2 selectivity, C_2 selectivity and oxygen permeation flux were defined as follows:

$$\mathrm{CH_4,\ conversion} = \frac{(F_{\mathrm{C_2H_4}} + F_{\mathrm{C_2H_6}})2 + F_{\mathrm{CO_2}} + F_{\mathrm{CO}}}{(F_{\mathrm{C_2H_4}} + F_{\mathrm{C_2H_6}})2 + F_{\mathrm{CO_2}} + F_{\mathrm{CO}} + F_{\mathrm{CH_4 outlet}}},$$

$$\mathrm{CO,\ selectivity} = \frac{F_{\mathrm{CO}}}{F_{\mathrm{CO}} + F_{\mathrm{CO_2}} + 2(F_{\mathrm{C_2H_4}} + F_{\mathrm{C_2H_6}})},$$

$$\mathrm{CO_2,\ selectivity} = \frac{F_{\mathrm{CO_2}}}{F_{\mathrm{CO}} + F_{\mathrm{CO_2}} + 2(F_{\mathrm{C_2H_4}} + F_{\mathrm{C_2H_6}})},$$

$$\mathrm{C_2,\ selectivity} = \frac{2(F_{\mathrm{C_2H_4}} + F_{\mathrm{C_2H_6}})}{F_{\mathrm{CO}} + F_{\mathrm{CO_2}} + 2(F_{\mathrm{C_2H_4}} + F_{\mathrm{C_2H_6}})},$$

$$J_{\mathrm{O_2}} = \frac{F_{\mathrm{CO}} + 2F_{\mathrm{CO_2}} + F_{\mathrm{H_2O}} + 2F_{\mathrm{O_2}}(\mathrm{unreacted})}{2S},$$

where S is the effective membrane surface of the reaction side.

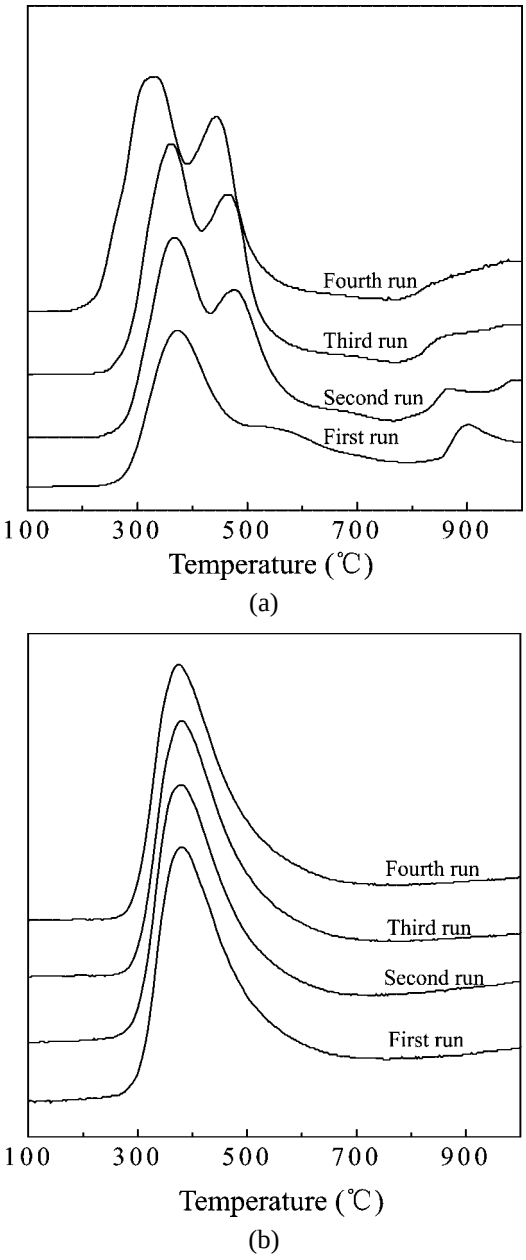

Figure 4. (a) Multi-run O_2-TPD profiles of SCFO. (b) Multi-run O_2-TPD profiles of BCFZO.

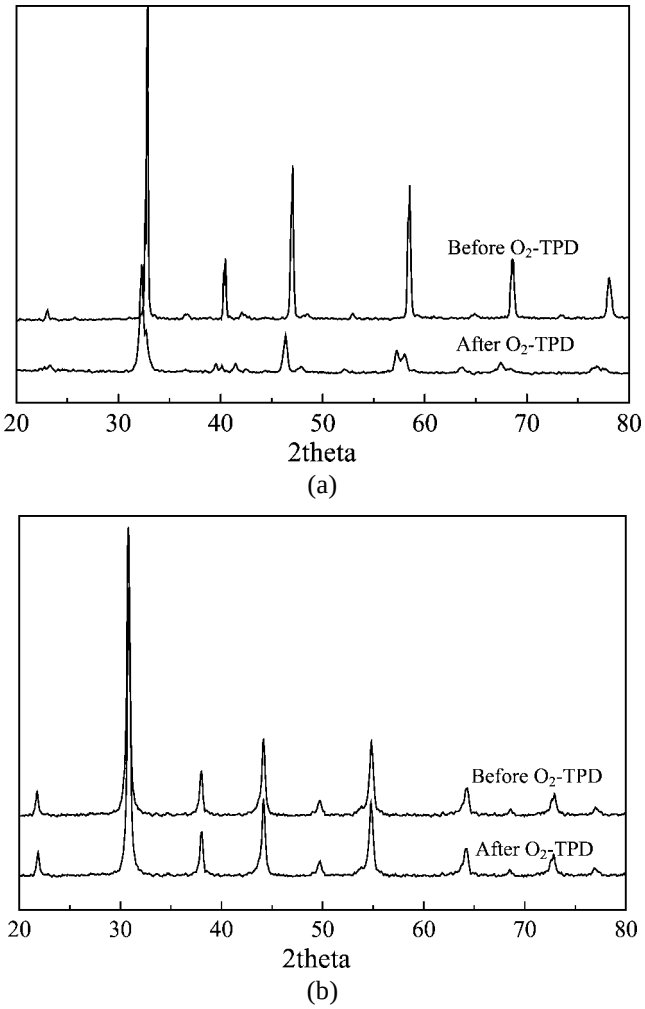

Figure 5. (a) XRD patterns of SCFO before and after O_2-TPD. (b) XRD patterns of BCFZO before and after O_2-TPD.

3. Results and discussion

3.1. Structural stability of SCFO and BCFZO

The structural stability of SCFO and BCFZO under inert atmosphere was characterized by multi-run O_2-TPD and XRD, as shown in figures 4 and 5, respectively. From figure 4(a) we could easily find that for SCFO the peak number, peak position and peak shape of different run oxygen desorption profiles were changed greatly, which revealed that SCFO had a low reversibility of oxygen adsorption and desorption. This was in accordance with the result of XRD shown in figure 5(a). The XRD patterns showed that the SCFO had a pure perovskite structure before the oxygen desorption experiment while after oxygen desorption new non-perovskite phases had emerged due to the loss of oxygen in the lattice. In comparison with SCFO, the profile of O_2-TPD for BCFZO (figure 4(b)) only possessed one oxygen desorption peak in the low-temperature zone from 300 to 700 °C. The desorption peak in the high-temperature zone corresponding to reduction of Co^{3+} ions and the large expansion of lattice parameters which could be seen for SCFO disappeared. This demonstrated that the introduction of Zr^{4+} made the reduction of Co^{3+} become more difficult, which denoted that the BCFZO material was relatively stable. In addition, a high reversibility of oxygen adsorption and desorption could be obtained and was consistent with the completely identical XRD patterns before and after the oxygen desorption experiment (figure 5(b)). The negligible small lattice expansion might be the reason why BCFZO possessed a stable structure under inert atmosphere. From the point of structural stability under inert atmosphere, BCFZO was more suitable for oxygen separation and supplying pure oxygen for the POM reaction.

The technique of H_2-TPR was used to characterize the structural stability of SCFO and BCFZO under a more reducing atmosphere. The XRD patterns after hydrogen re-

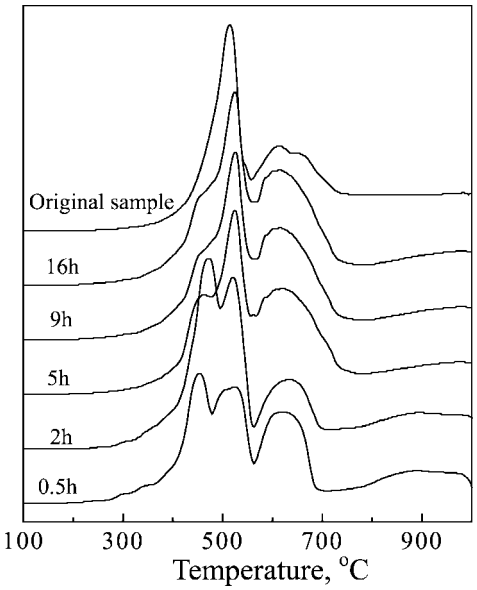

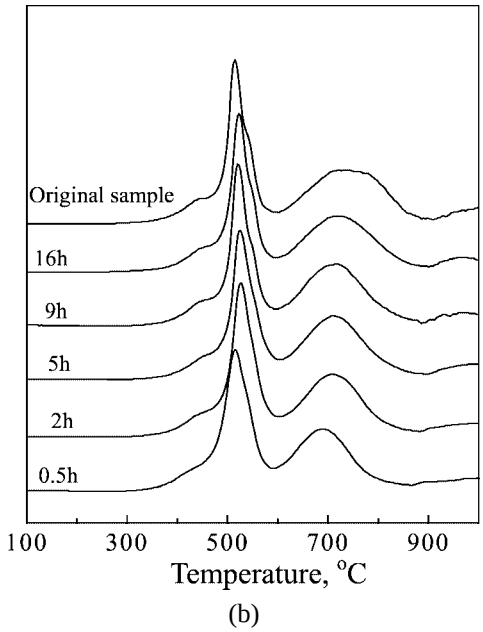

Figure 6. (a) Multi-run H_2-TPR profiles of SCFO after recovery at 800 °C for different times. (b) Multi-run H_2-TPR profiles of BCFZO after recovery at 800 °C for different time.

duction showed that both SCFO and BCFZO did not maintain the pure perovskite structure. Therefore, the mixture of 1% O_2 and 99% Ar was used to recovery the original pure perovskite structure for SCFO and BCFZO. Figure 6 (a) and (b) have given the multi-run H_2-TPR profiles of SCFO and BCFZO after recovery for different times at 800 °C. It was very clear that the long-term recovery of 16 h could not give an identical H_2-TPR profile as the original one for SCFO, while only 0.5 h was long enough for BCFZO to recover its original structure and to give an identical H_2-TPR profile as the first run H_2-TPR profile. The XRD patterns of SCFO recovery for 16 h and of BCFZO recovery for 0.5 h were displayed in figure 7, which proved that BCFZO could

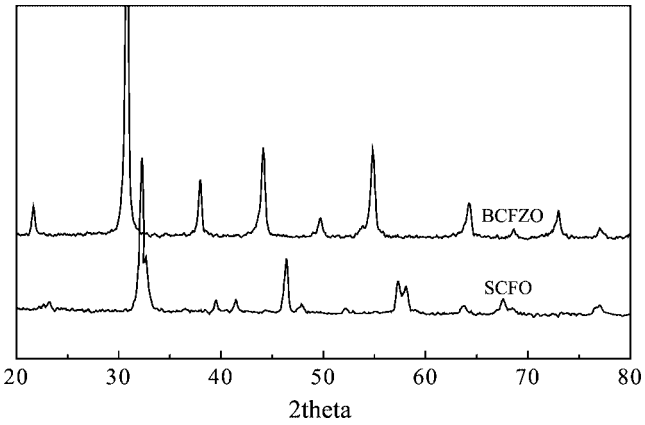

Figure 7. XRD patterns of SCFO and BCFZO after performing the H_2-TPR experiment and then recovery in 1% O_2 + 99% Ar for 16 h and 0.5 h, respectively.

more easily recover its original structure than SCFO. The reversible structure of BCFZO under a more reducing atmosphere made it more suitable for constructing POM reactors than SCFO.

3.2. Oxygen permeability under air/He gradient

The temperature dependence of the oxygen permeation flux of Arrhenius form through SCFO and BCFZO membrane disks is shown in figure 8. The fluxes of these two membrane disks were very high and increased rapidly with increase in temperature. This resulted from the elevation of the oxygen vacancy diffusion rate in the bulk lattice and the elevation of the surface oxygen and oxygen ion exchange rate with the increase in temperature. A slightly higher permeation flux was found for SCFO than for BCFZO. But the activation energy for oxygen permeation for SCFO was also higher than that of BCFZO. In addition, two activation energies corresponding to different phase structures in the temperature range of 600–950 °C were found for SCFO. As for BCFZO, we could only see a single activation energy, which showed that the cubic perovskite structure was kept

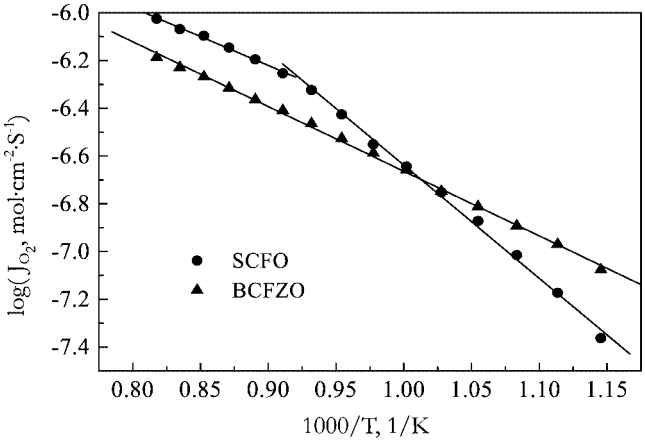

Figure 8. The Arrhenius plots for oxygen permeation of SCFO and BCFZO membrane disks under air/He gradient, air flux 150 m min^{-1}, He flux 30 ml min^{-1}, thickness 1.0 mm.

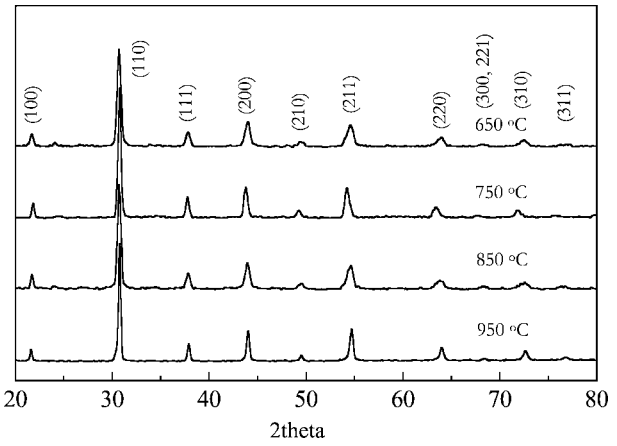

Figure 9. XRD patterns of BCFZO after treatment in high purity helium for 100 h at different temperatures.

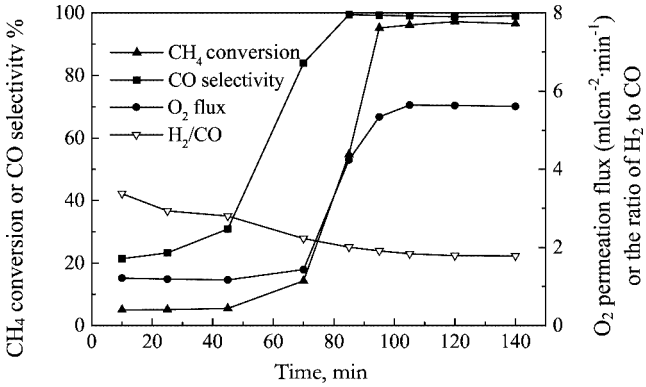

Figure 10. Initiation stage of the BCFZO MIECM reactor for the POM reaction.

well in the range of 600–950 °C. The identical cubic perovskite structures were demonstrated by treating the samples in pure helium at different temperature for 100 h and then immediately submitting these samples to XRD characterization. Figure 9 gives the XRD patterns of BCFZO after treatment at 650, 750, 850 and 950 °C, which revealed that the cubic perovskite structure was well preserved.

3.3. POM reaction in membrane reactors constructed from SCFO and BCFZO

The performance of SCFO and BCFZO membrane reactors was investigated using the reactor configuration shown in figure 3. SCFO membrane disks survived only a few hours when operated as a reactor for the POM reaction at 850 °C. The abrupt cracking of the disks led to an interruption of this reactor. This was in accordance with the unstable structure and unsteady oxygen permeability of SCFO under inert atmosphere discussed above. As for the BCFZO reactor, the POM reaction was performed successfully for a long time and good performance was obtained.

The time dependence of the oxygen permeation flux and catalytic performance of the BCFZO membrane reactor during the induction period are shown in figure 10. At the beginning ($t = 10$ min), the oxygen permeation flux was twice as high as that under air/He gradient. This might have resulted from the slightly lower oxygen partial pressure in the mixture of He CH_4, CO, CO_2 and H_2 than the original helium atmosphere and the contribution of dual-phase permeation caused by the gold ring and membrane disk. The CH_4 conversion was only around 5%, and the main carbon-containing products were CO_2 (∼80%) and CO (∼20%). The ratio of H_2 to CO was higher than 2. With the increase of the induction time, the oxygen permeation flux, the CH_4 conversion and the CO selectivity increased modestly. When the induction time exceeded 40 min, the CO selectivity improved very quickly, at $t = 80$ min nearly 100% CO selectivity had been achieved. The abrupt increase of oxygen permeation flux and CH_4 conversion was a little delayed, which began at $t = 70$ min and finished at $t = 100$ min. Within 120 min, a CH_4 conversion of 96–98%, a CO selectivity of 98–99%, an oxygen permeation flux of around 5.4–5.8 ml cm^{-2} min^{-1} (1.9–2.0 μmol m^{-2} S^{-1} Pa^{-1}) and a proper ratio of H_2 to CO close to 2 were achieved. The above phenomena could be interpreted by the factor of the activation of the catalyst and the structure adjustment of the membrane. At the beginning, the activation of the catalyst was the rate-determining step. In the fresh catalyst used in this study, the nickel was in the oxidation state, *i.e.*, $NiAlO_4$, which was active for methane combustion. This might give a good reason why the CO_2 selectivity was very high at the beginning. The initial reduction of $NiAlO_4$ to Ni^0 was somewhat difficult, but once some Ni^0 appeared, the reduction process was accelerated by the produced H_2 and CO. The reduction of $NiAlO_4$ to Ni^0 and the production of H_2 and CO accelerated each other, which resulted in the rapid increase of the CO selectivity and the H_2 selectivity. The induction of the LiLaNiO/γ-Al_2O_3 catalyst was finished within 60 min, which was in accordance with the induction in the conventional co-fed reactor. After the induction of the catalyst, the structure adjustment of the membrane became the rate-determining step. The rate of structure adjustment varied greatly for different membrane materials. As for the BCZFO studied in our experiment, the structure adjustment was very quick and only a small change occurred on the membrane surface. The original bulk lattice was suitable for high oxygen permeability, and was not adjusted, which has been proved by the structure analysis of the membrane after long-term operation of the POM reaction. Therefore, the oxygen permeation flux and the CH_4 conversion sharply increased after the induction of the catalyst. And because the CH_4 conversion and the oxygen permeation flux accelerated each other, they possessed an abrupt increase between $t = 70$ and 100 min. As for $Ba_{0.5}Sr_{0.5}Co_{0.8}Fe_{0.2}O_{3-\delta}$ (BSCFO) [15] and $La_{0.2}Ba_{0.8}Co_{0.2}Fe_{0.8}O_{3-\delta}$ (LBCFO) [11] reactors, the structure adjustment was relatively difficult, which resulted in the longer induction period of these two reactors. For the BSCFO reactor, the induction period ended within 20 h, whilst for LBCFO, 500 h was needed to reach the operational steady state.

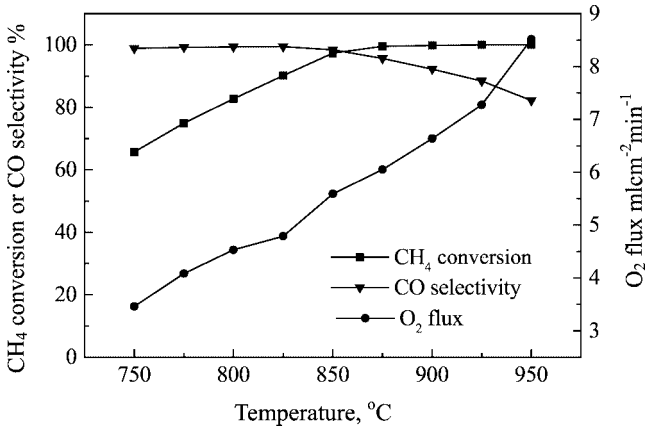

Figure 11. Effects of temperature on the CH_4 conversion, CO selectivity and O_2 permeation flux.

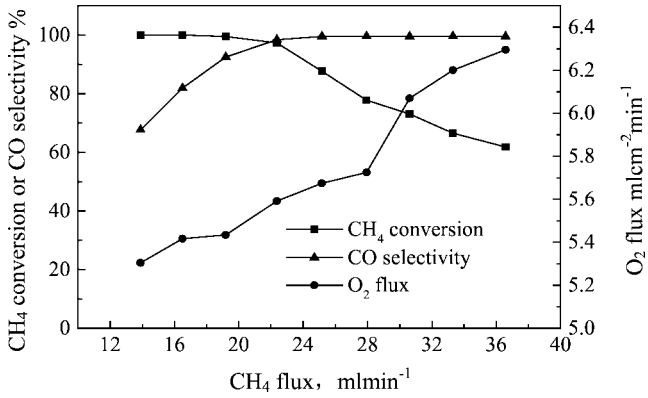

Figure 12. Effects of CH_4 flux on the CH_4 conversion, CO selectivity and O_2 permeation flux.

Figure 11 shows the temperature dependence of CH_4 conversion, CO selectivity and oxygen permeation flux with 50% helium diluted methane at a flow rate of 24 $ml\,min^{-1}$ and air at a flow rate of 150 $ml\,min^{-1}$. The CH_4 conversion and oxygen permeation flux increased rapidly with the increase in temperature and the CO selectivity decreased slowly in contrast. The elevating of the oxygen permeation flux was due to enhancing of the diffusion rate of oxygen vacancy *via* the bulk lattice and the enhancing of the surface exchange rate with increasing operational temperature, which was identical with the results obtained under the air/He gradient. For an excess feed of methane, the CH_4 conversion efficiency was mainly controlled by the oxygen permeation flux and the increase in oxygen permeation flux spontaneously led to the increase in the methane conversion. When methane was kept in excess, the CO selectivity was unchanged and near 100%. But with the increase of oxygen permeation flux, the oxygen was in excess and the deep oxidation of CO took place and the CO selectivity decreased slowly. At 950 °C, an oxygen permeation of 8.6 $ml\,cm^{-2}\,min^{-1}$ (3.0 $\mu mol\,m^{-2}\,S^{-1}\,Pa^{-1}$) and CH_4 conversion of nearly 100% were obtained, while the CO selectivity only was 82%. At 850 °C, not only the high oxygen permeation flux of 5.6 $ml\,cm^{-2}\,min^{-1}$ (1.96 $\mu mol\,m^{-2}\,S^{-1}\,Pa^{-1}$) and the high CH_4 conversion of 97.5% were achieved, but also the high CO selectivity of 98.5% was obtained.

Figure 12 shows the methane flux dependence of oxygen permeation flux, CH_4 conversion and CO selectivity when the operational temperature was unchanged at 850 °C. At first, the CO selectivity and oxygen permeation flux increased rapidly with increasing methane flux and the methane conversion decreased slowly in contrast. When the methane flux was 24 $ml\,min^{-1}$, the high CH_4 conversion of 97.5%, the high CO selectivity of 98.5% and the oxygen permeation flux of 5.6 $ml\,cm^{-2}\,min^{-1}$ (1.96 $\mu mol\,m^{-2}\,S^{-1}\,Pa^{-1}$) were achieved. With the continuous increase of the methane flux, the CH_4 conversion rapidly decreased. Meanwhile, the oxygen permeation flux was still increasing and the CO selectivity kept unchanged around 99%. The changes of CH_4 conversion and the CO selectivity with the methane flux could be interpreted by the POM reaction performance under different ratios of CH_4 to O_2 as in a conventional co-fed reactor. The low ratio of CH_4 and O_2 was responsible for the deep oxidation of methane and the low CO selectivity and high methane conversion. The high ratio of CH_4 and O_2 was responsible for the partial oxidation of methane and high CO selectivity and low methane conversion. Only when the ratio of CH_4 and O_2 was around 2 could good performance be achieved. The continuous increase of oxygen permeation flux resulted from the decrease of oxygen partial pressure caused by the increase of the tail flux and the yield of CO and H_2.

Figure 13 shows the long-term stability of the BCFZO membrane reactor for the POM reaction. After a short induction period of 2 h, CH_4 conversion of 96–98%, CO selectivity of 98–99%, oxygen permeation flux around 5.4–5.8 $ml\,cm^{-2}\,min^{-1}$ (1.9–2.0 $\mu mol\,m^{-2}\,S^{-1}\,Pa^{-1}$) and a proper ratio of H_2 to CO close to 2 were achieved. During a more than 2200 h running, the oxygen permeation flux was fairly stable, similar to the stable reaction performance of CH_4 conversion, CO selectivity and the ratio of H_2 to CO. And there was an important point we should stress, namely, the ending of this experiment in the BCFZO reactor was caused by an abrupt failure of the power supply, and not due

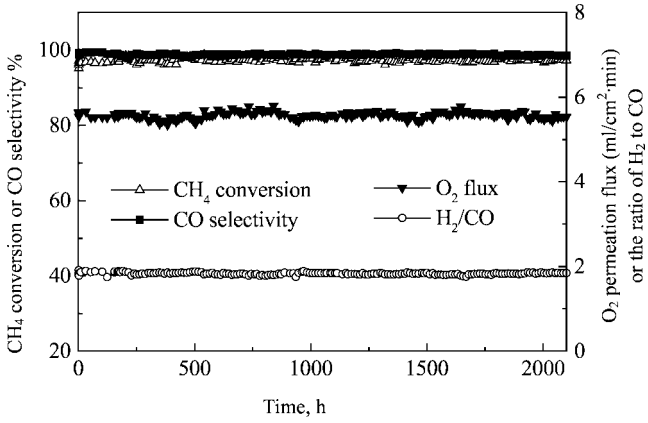

Figure 13. Long-term stability of the BCFZO membrane reactor at 850 °C for the POM reaction.

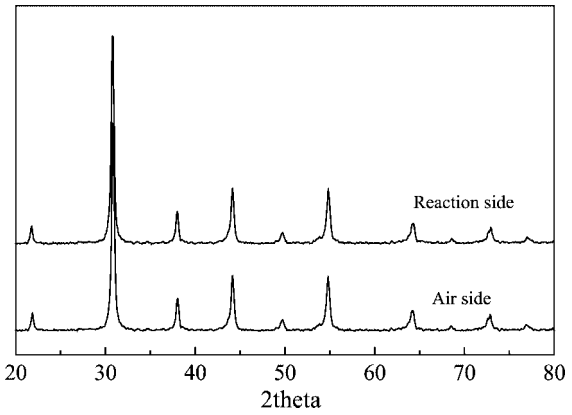

Figure 14. XRD patterns of the long-term reaction membrane after removal of the surface layers.

to the failure of the reactor. This long-term stable operation showed that the BCFZO membrane reactor was more stable than any other mixed conducting membrane reactors for the POM reaction published so far, except for that constructed from $Sr_{1.7}La_{0.3}Ga_{0.6}Fe_{1.4}O_{5.15}$ (SLGFO) [19]. But it was well known that not only the gallium element was more expensive but also its oxygen permeation flux was too low to be suitable for practical application. These two shortcomings made SLGFO not suitable for constructing a reactor for the POM reaction, when compared with the new material of BCFZO developed by us.

In order to interpret why the BCFZO membrane reactor had a very stable POM reaction performance, the membrane disk after the long-term reaction was subjected to characterization by techniques of XRD, EDS and XPS. The XRD patterns of both the reaction side and the air side of the membrane disk showed that the cubic perovskite structure has been destroyed and the metal oxides and carbonates have been formed on both top layers, which might be a result of the structure adjustment in the induction period of the membrane reactor. After the other characterization the surface layers of both top layers were removed and the disk was submitted to XRD again. The XRD patterns shown in figure 14 indicated that the cubic perovskite structure was still kept unchanged. This might be one reason why the membrane disk could operate steadily for a long time. This result was accompanied by the unchanged element composition in the membrane bulk lattice obtained by EDS analysis (figure 15). Another factor to determine the stability of the BCFZO membrane reactor was the interaction between the membrane and the catalyst. The solid-state reaction between membrane surface and the catalyst could form a new phase that impairs the oxygen permeability and POM reaction performance. The reaction could diffuse into the membrane bulk lattice and result in the failure of the membrane reactor eventually. The BSCFO membrane reactor, which had high oxygen permeability and good reaction performance, only steadily operated for 500 h for this reason [15]. But the profiles of the XPS and EDS of the reaction side of the BCFZO membrane after long-term reaction (shown in figures 16 and 17) indicated that no elements of the LiLaNiO/γ-Al_2O_3 catalyst were found. There did not exist the solid-state reaction between the membrane and the catalyst, which might be another reason why the BCFZO membrane reaction could

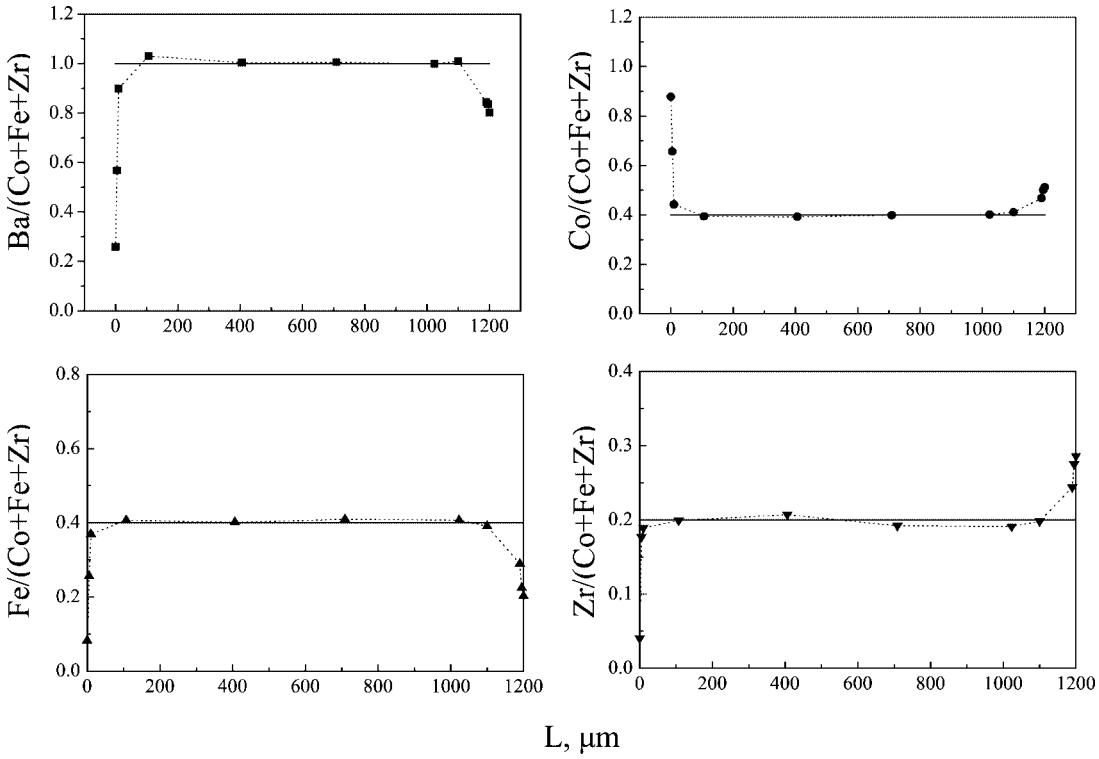

Figure 15. Crosswise EDS composition analyses Atomic ratio vs. the depth of membrane from the reduction-side surface ($L = 0$ μm) to the air-side surface ($L = 1200$ μm).

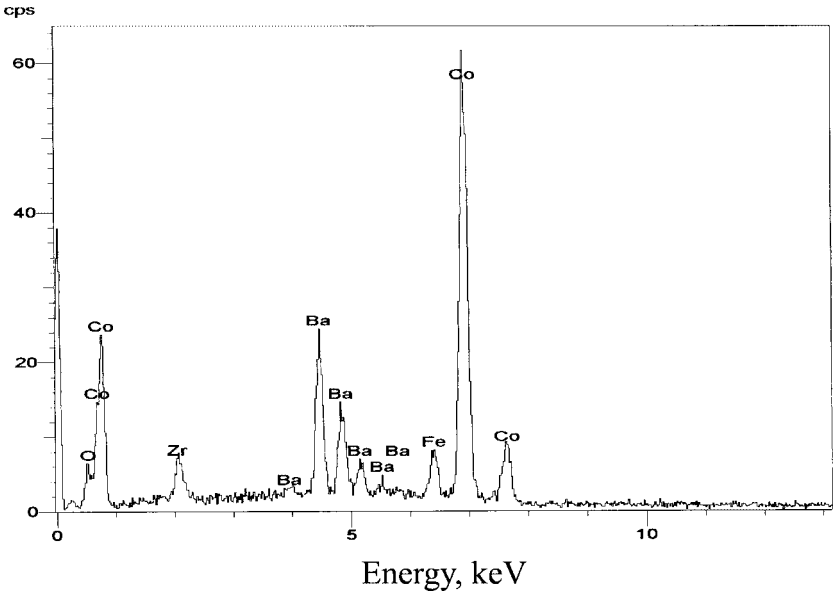

Figure 16. EDS profiles of reaction side of BCFZO membrane disk after long-term POM reaction.

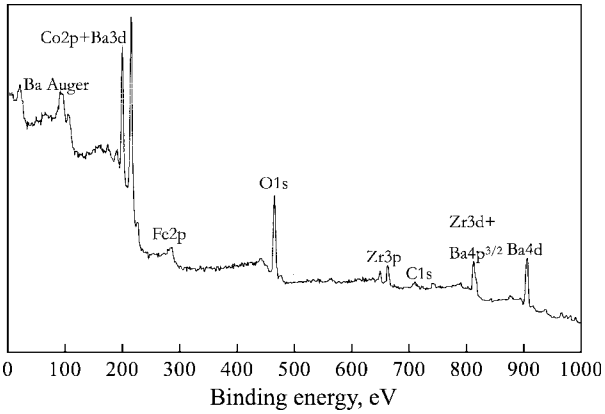

Figure 17. XPS profiles of reaction of BCFZO membrane disk subsequent to long-term POM reaction.

steadily operate for a long time, more than 2200 h. From the point of long-term steady operation, the BCFZO membrane reactor was more suitable for the POM reaction.

In conclusion, a novel zirconium-based perovskite type material of BCFZO for constructing membrane reactors for the POM reaction was synthesized. The high structural stability and oxygen permeation flux were evidenced by XRD, O_2-TPD results and oxygen permeation studies. Moreover, long-term stability was evidenced through the running of the POM reaction for more than 2200 h. Not only high oxygen permeability and excellent catalytic performance for the POM reaction were obtained, but also an induction period shorter than any other MIECM materials published so far was achieved.

Acknowledgment

The authors gratefully acknowledge the financial support of the National Natural Science Foundation of China (Grant No. 59789201), the National Advanced Materials Committee of China (Grant No. 715-006-0122) and the Ministry of Science and Technology, China (Grant No. G1999022401)

References

[1] Y. Amenomiya, V.I. Buss, M. Goledzinszka and A.R. Sanger, Catal. Rev. Sci. Eng. 32 (1990) 163.
[2] A.T. Ashcroft, A.K. Cheetham, J.S. Foord, M.L.H. Green, C.P. Grey, A.J. Murrell and P.D.F. Vernon, Nature 344 (1990) 319.
[3] W.J.M. Vermeiren, E. Blomsma and P.A. Jacobs, Catal. Today 13 (1992) 427.
[4] D.A. Hickman and L.D. Schmidt, Science 259 (1993) 343.
[5] R.F. Blanks, T.S. Wittrin and D.A. Peterson, Chem. Eng. Sci. 45 (1990) 2407.
[6] E. Supp, in: *Proc. World Methanol Conference*, Houston, TX (1989).
[7] Y. Teraoka, H.M. Zhang, S. Furukawa and N. Yamazoe, Chem. Lett. 167 (1985) 1743.
[8] Y. Teraoka, T. Nobunaga and N. Yamazoe, Chem. Lett. 195 (1988) 503.
[9] Y. Teraoka, T. Nounaga, K. Okamoto, N. Miura and N. Yamazoe, Solid State Ionics 48 (1991) 207.
[10] U. Balachandran, J.T. Dusek, P.S. Maiya, B. Ma, R.L. Mieville, M.S. Kleefisch and C.A. Udovich, Catal. Today 36 (1995) 265.
[11] C.Y. Tsai, A.G. Dixon, W.R. Moser and Y.H. Ma, AIChE J. (Ceramics Processing) 43(11A) (1997) 2741.
[12] M. Schwartz, J.H. White and A.F. Sammells, Int. Patent, WO 99/21649 (1999).
[13] Z.P. Shao, G.X. Xiong, Y. Cong and W.S. Yang, J. Membr. Sci. 164 (2000) 167.
[14] Z.P. Shao, W.S. Yang, Y. Cong, H. Dong, J.H. Tong and G.X. Xiong, J. Membr. Sci. 172 (2000) 177.
[15] Z.P. Shao, H. Dong, G.X. Xiong, Y. Cong and W.S. Yang, J. Membr. Sci. 183 (2001) 181.
[16] M. Matsui, T. Soma and I. Oda, J. Amer. Ceram. Soc. 69 (1986) 198.
[17] A.G. Evans and K.T. Faber, J. Am. Ceram. Soc. 67 (1984) 255.
[18] S.L. Liu, G.X. Xiong, S.S. Sheng et al., Stud. Surf. Sci. Catal. 119 (1998) 747.
[19] M. Schwartz, J.H. White and A.F. Sammells, Int. Patent, WO 99/21649 (1999).